Published in final edited form as:

ACS Chem Neurosci. 2021 October 06; 12(19): 3733–3744. doi:10.1021/acschemneuro.1c00492.

In Vitro and *In Vivo* Investigation of S1PR1 Expression in the Central Nervous System Using [^{3}H]CS1P1 and [^{11}C]CS1P1

Hao Jiang,
Department of Radiology, Washington University School of Medicine, St Louis, Missouri 63110, United States

Sumit Joshi,
Department of Radiology, Washington University School of Medicine, St Louis, Missouri 63110, United States

Hui Liu,
Department of Radiology, Washington University School of Medicine, St Louis, Missouri 63110, United States

Syahir Mansor,
Department of Radiology, Washington University School of Medicine, St Louis, Missouri 63110, United States

Lin Qiu,
Department of Radiology, Washington University School of Medicine, St Louis, Missouri 63110, United States

Haiyang Zhao,
Department of Radiology, Washington University School of Medicine, St Louis, Missouri 63110, United States

Timothy Whitehead,
Department of Radiology, Washington University School of Medicine, St Louis, Missouri 63110, United States

Robert J. Gropler,
Department of Radiology, Washington University School of Medicine, St Louis, Missouri 63110, United States

Gregory F. Wu,

Corresponding Author: **Zhude Tu –** Department of Radiology, Washington University School of Medicine, St Louis, Missouri 63110, United States; Phone: 314-362-8487; zhudetu@wustl.edu; Fax: 314-362-8555.

Author Contributions

H.J., S.J., H.L., and Z.T. conceived the project and designed the experiments. H.J., S.J., H.L., S.M., L.Q., H.Z., and T.W. performed the experiments and data analysis. H.J., H.L., and Z.T. wrote the manuscript. All authors edited and approved the manuscript.

Supporting Information

The Supporting Information is available free of charge at https://pubs.acs.org/doi/10.1021/acschemneuro.1c00492.
In vitro autoradiography of [^{3}H]CS1P1 and immunostaining of S1PR1 in the rat brain; *in vitro* autoradiography of [^{3}H]CS1P1 and immunostaining of S1PR1 in the human cerebellum; and *in vivo* microPET uptake of [^{11}C]CS1P1 in rat and different regions of spinal cords (PDF)

Complete contact information is available at: https://pubs.acs.org/10.1021/acschemneuro.1c00492

The authors declare no competing financial interest.

Department of Neurology, Washington University School of Medicine, St Louis, Missouri 63110, United States

Anne H. Cross,
Department of Neurology, Washington University School of Medicine, St Louis, Missouri 63110, United States

Tammie L. S. Benzinger,
Department of Radiology, Washington University School of Medicine, St Louis, Missouri 63110, United States; Department of Neurological Surgery, Washington University School of Medicine, St Louis, Missouri 63110, United States

Kooresh I. Shoghi,
Department of Radiology, Washington University School of Medicine, St Louis, Missouri 63110, United States

Joel S. Perlmutter,
Department of Radiology, Washington University School of Medicine, St Louis, Missouri 63110, United States; Department of Neurology, Washington University School of Medicine, St Louis, Missouri 63110, United States

Zhude Tu
Department of Radiology, Washington University School of Medicine, St Louis, Missouri 63110, United States;

Abstract

Sphingosine-1-phosphate receptor 1 (S1PR1) is ubiquitously expressed among all tissues and plays key roles in many physiological and cellular processes. In the central nervous system (CNS), S1PR1 is expressed in different types of cells including neurons, astrocytes, and oligodendrocyte precursor cells. S1PR1 has been recognized as a novel therapeutic target in multiple sclerosis and other diseases. We previously reported a promising S1PR1-specific radioligand, [^{11}C]CS1P1 (previously named [^{11}C]TZ3321), which is under clinical investigation for human use. In the current study, we performed a detailed characterization of [^{3}H]CS1P1 for its binding specificity to S1PR1 in CNS using autoradiography and immunohistochemistry in human and rat CNS tissues. Our data indicate that [^{3}H]CS1P1 binds to S1PR1 in human frontal cortex tissue with a K_d of 3.98 nM and a B_{max} of 172.5 nM. The distribution of [^{3}H]CS1P1 in human and rat CNS tissues is consistent with the distribution of S1PR1 detected by immunohistochemistry studies. Our microPET studies of [^{11}C]CS1P1 in a nonhuman primate (NHP) show a standardized uptake value of 2.4 in the NHP brain, with test–retest variability of 0.23% among six different NHPs. Radiometabolite analysis in the plasma samples of NHP and rat, as well as in rat brain samples, showed that [^{11}C]CS1P1 was stable *in vivo*. Kinetic modeling studies using a two-compartment tissue model showed that the positron emission tomography (PET) data fit the model well. Overall, our study provides a detailed characterization of [^{3}H]CS1P1 binding to S1PR1 in the CNS. Combined with our microPET studies in the NHP brain, our data suggest that [^{11}C]CS1P1 is a promising radioligand for PET imaging of S1PR1 in the CNS.

Graphical Abstract

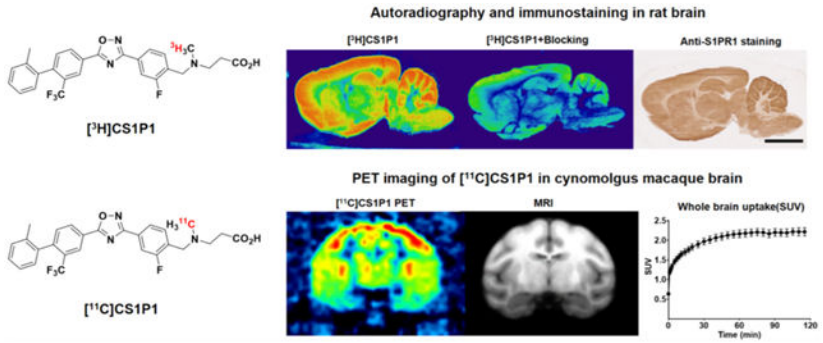

Keywords

sphingosine-1-phosphate receptor 1; central nervous system; positron emission tomography; [^{3}H]CS1P1 autoradiography; [^{11}C]CS1P1 PET imaging; radiopharmaceutical

INTRODUCTION

Sphingosine-1-phosphate (S1P) is a bioactive lipid mediator that can affect many physiological and cellular processes through a five-member family of G protein-coupled S1P receptors (S1PR1–5). Numerous studies demonstrate that the S1P-S1PR pathway plays an important role in various pathophysiological processes, such as angiogenesis,[1] neurodegeneration,[2] and immune responses.[3] The S1P-S1PR pathway has been recognized as a therapeutic target in diverse diseases. FTY720 (fingolimod), for example, is a well-characterized functional antagonist of S1PRs approved by the FDA for treating relapsing multiple sclerosis (MS).[4,5]

Among all S1PRs, S1PR1 is the most abundant S1P receptor that is ubiquitously expressed throughout all tissues, including the central nervous system (CNS).[6] Intriguingly, numerous studies demonstrate that S1PR1 is involved in many physiological and cellular processes in the CNS. For example, activation of S1PR1 in neural stem cells is involved in neurogenesis and neurocognitive recovery following traumatic brain injury;[7] S1PR1 activation in astrocytes contributes to neuropathic pain;[8] and the S1PR1/STAT3 axis in the hypothalamus is important for energy homeostasis.[9] More importantly, recent studies also indicate that S1PR1 is directly involved in neuroimmune responses, playing a critical role in the neuroinflammatory disease MS. Previous studies reported that S1PR1 is upregulated in active and chronic inactive MS lesions,[10] and the S1PR1/STAT3 axis directly contributes to the severity of neuroinflammation in an animal model of MS.[11] Although S1PR1 is important in the CNS and is considered a promising therapeutic target in many neurological disorders, the precise distribution and function of S1PR1, particularly of activated S1PR1, in the human CNS remain not well understood.

Given the importance of S1PR1 in the CNS, positron emission tomography (PET) with a specific S1PR1 radioligand could offer a powerful non-invasive methodology to quantitatively measure S1PR1 expression levels *in vivo* and to evaluate the target engagement and therapeutic response of S1PR1-targeting drugs. Our previous studies

indicated that the ligand CS1P1 has a high binding affinity toward S1PR1 with an IC_{50} value of 2.13 nM and more than 1000-fold selectivity over other S1PRs.[12] We previously reported the methodology for radiosynthesis of [^{11}C]CS1P1 (previously named [^{11}C]-TZ3321) and evaluation of [^{11}C]CS1P1 using three rodent models of human disease including vascular injury,[12] atherosclerosis,[13] and MS;[14] and our data indicated that [^{11}C]CS1P1 is a promising radiotracer for investigating S1PR1 function *in vivo*. In fact, with the FDA approval for an exploratory investigational new drug (eIND) study in human, clinical investigation of [^{11}C]CS1P1 in normal healthy volunteers to determine its safety and distribution in human subjects, as well as proof of mechanism in patients with MS, is in progress at our institution.

To further illustrate the distribution of S1PR1 in CNS, as well as to characterize the radioligand [^{11}C]CS1P1 in the CNS, we performed detailed studies using a tritiated analogue of [^{11}C]CS1P1 and [^{3}H]CS1P1 in the CNS. We investigated the expression pattern of activated S1PR1 using an *in vitro* autoradiograph study with [^{3}H]CS1P1 and an immunohistochemistry staining study in rodent brain and spinal cords, as well as various regions of postmortem human brain tissues. We also performed microPET brain imaging studies of [^{11}C]CS1P1 in six macaques and rats brain and spinal cords. Our studies indicate that CS1P1 is a promising radioligand for PET imaging studies of S1P1 function in CNS.

RESULTS

Saturation and Competition Binding Study Using the Recombinant Human S1PR1 Membrane.

To facilitate the *in vitro* validation of the CS1P1 radioligand, in this study, we first used [^{3}H]CS1P1, sharing the exact same molecular structure with [^{11}C]CS1P1 but radiolabeled with a different isotope (Figure 1A) to perform saturation binding assays and radioligand competition binding studies with recombinant human S1PR1 (hS1PR1) membranes (Figure 1B–D). Saturation binding data showed that [^{3}H]CS1P1 had high potency in binding to hS1PR1 with a K_d value of 8.41 ± 1.43 nM and B_{max} of 4156 ± 140.7 fmol/mg (Figure 1B,C). In the competition binding assay, the relative affinities of the endogenous S1PR ligand S1P and other known S1PR1 compounds with [^{3}H]CS1P1 were compared using recombinant hS1PR1 membranes. Among tested compounds, FTY720-(S)-P and S1P displaced [^{3}H]CS1P1 with a K_i value of 4.5 and 5.7 nM respectively, indicating that [^{3}H]CS1P1 binding to hS1PR1 could compete with S1PR1 potent compounds FTY720(S)-P. However, for the S1PR1 antagonist SEW2871, displacement studies with [^{3}H]CS1P1 showed a relatively lower K_i value of 354 nM (Figure 1D). These data along with our previous studies confirmed that ligand CS1P1 has high potency and specificity in binding to S1PR1.

In Vitro Saturation Autoradiography Study in the Rat Brain and Human Frontal Cortex.

In addition to radioligand binding assays with the recombinant hS1PR1 membranes, we next performed saturation autoradiography studies in the rat and human brain tissues (Figure 1E–I). For the rat brain cortex region, [^{3}H]CS1P1 bound to S1PR1 with a K_d of 2.25 ± 0.41 nM, a B_{max} of 134.6 ± 6.69 nM, and a B_{max}/K_d ratio of 59.8 (Figure 1E). For the rat brain hippocampus region, [^{3}H]CS1P1 bound to S1PR1 with a K_d of 2.81 ± 0.42 nM, a B_{max} of

144.5 ± 6.22 nM, and a B_{max}/K_d ratio of 51.4 (Figure 1F). For the gray matter region of the human frontal cortex, [^{3}H]CS1P1 bound to S1PR1 with a K_d of 3.98 ± 0.52 nM, a B_{max} of 172.5 ± 7.13 nM, and the ratio of B_{max}/K_d was 43.3 (Figure 1G).

In Vitro Characterization of [^{3}H]CS1P1 in the Rat Brain and Spinal Cord.

We then characterized the distribution of [^{3}H]CS1P1 and S1PR1 expression in the rat brain and spinal cord (Figure 2). Both autoradiograph and immunostaining studies indicated that [^{3}H]CS1P1 and S1PR1 were mainly distributed in gray matter throughout the rat brain and spinal cord; the radioactivity of [^{3}H]CS1P1 was blocked by NIBR-0213 as expected, and the distribution of [^{3}H]CS1P1 matched well with anti-S1PR1 staining (Figure 2A,B). For the rat brain, the level of S1PR1 was relatively high in the cortex, hippocampus, striatum, thalamus, and hypothalamus, while a very low level of S1PR1 was observed in the corpus callosum and internal capsule (Figures 2A,B, S1). In the rat cerebellum, similar to the human brain, the level of S1PR1 was relatively high in the molecular layer compared with the granular layer (Figures 2B, S1). For the rat spinal cord, [^{3}H]CS1P1 and S1PR1 were also mainly located in the gray matter (Figure 2C), and the region of pyramidal decussation is highlighted in Figure S1E. We also carried out a semiquantitative comparison of [^{3}H]CS1P1 in different rat brain regions. In general, [^{3}H]CS1P1 in the cerebellar cortex was about 4-fold higher than that in cerebellar white matter. Cortex, hippocampus, hypothalamus, and cerebellar cortex had the highest [^{3}H]CS1P1 intensity, whereas the corpus callosum, pons, and cerebellar white matter had the lowest intensity (Figures 2D, S1).

Distribution of [^{3}H]CS1P1 and the S1PR1 in Various Regions of the Human Brain.

In addition to the rat brain and spinal cord, we also performed *in vitro* autoradiography studies and immunostaining studies in various regions of fresh frozen post-mortem human brain tissues. Both autoradiograph and immunostaining studies indicated that [^{3}H]CS1P1 and S1PR1 were distributed mainly in the gray matter region throughout the brain with no to very low amounts in the white matter regions (Figure 3). For the frontal cortex of human brain tissue, similar to the immunostaining study using anti-S1PR1 antibody, the radioactivity signal of [^{3}H]CS1P1 was much stronger in the gray matter than that in the white matter [Figure 3A(i,iii)]; meanwhile, the S1PR1-specific antagonist, NIBR-0213 was able to block [^{3}H]CS1P1 well [Figure 3A(ii)], indicating that [^{3}H]CS1P1 binds with S1PR1 specifically. In the cerebellar region of the human brain, both autoradiography and immunostaining showed a high level of S1PR1 in the gray matter and the dentate nucleus (Figures 3B, S2B). In particular, the expression level of S1PR1 in the molecular layer of the cerebellar cortex was higher than that in the granular layer (Figure S2C). In the human striatal region, S1PR1 distributed mainly in the putamen and caudate nucleus with much lower expression levels in the internal capsule region (Figure 3C). In the midbrain region of the human brain, the expression level of S1PR1 was relatively high in the red nucleus region and very low in the cerebral peduncles and substantia nigra (Figure 3D). In the thalamus region of the human brain, both autoradiography and immunostaining showed that S1PR1 was relatively high in the anterior thalamus region but low in the internal capsule region (Figure 3E).

MicroPET Brain Study of [^{11}C]CS1P1 in Cynomolgus Macaques.

To further characterize our S1PR1-specific ligand CS1P1 in the CNS, particularly in living subjects, we performed microPET studies in the brains of cynomolgus macaques using our leading FDA-approved radioligand [^{11}C]CS1P1. In general, the uptake of [^{11}C]CS1P1 was relatively high in the macaques' brain with a standardized uptake value (SUV) of ~2.4. The tracer entered the brain quickly after the injection, peaked at ~60 min, and remained at the same level until 120 min (Figure 4A). Notably, though our tracer can reach a transient equilibrium in 60 min, no significant washout was identified until 120 min, indicating that this radiotracer tracer has a relatively slow washout pharmacokinetics.

After the uptake of [^{11}C]CS1P1 peaked in the brain, the brain regions including the striatum (caudate and putamen), prefrontal cortex, and the thalamus displayed a high uptake of tracer, the highest uptake (SUV) reached ~3.0 in the thalamus at 100 min post injection. Meanwhile, the brain regions, including basal frontal cortex, medial temporal lobe, and cortical white matter, displayed relatively lower tracer uptake, and the lowest tracer uptake (SUV) was ~1.1 in the cortical white matter at 100 min post injection (Figure 4B–D). The distribution of [^{11}C]CS1P1 in the brain is consistent with our autoradiograph and immunostaining studies of the brain regions from human post mortem brain tissues, indicating that S1PR1 is mainly distributed in the gray matter throughout the brain.

Test–retest reproducibility measurment of microPET brain scans were also performed in six macaques to examine the reproducibility and to establish the baseline level of [^{11}C]CS1P1 in the macaque brain. Our data showed that the brain uptake among different animals was consistent with minimal variability (Figure 4A). The average difference of test–retest mean SUV was 0.9%, and the test–retest variability (TRV) was 0.23%, suggesting that PET measurement of [^{11}C]CS1P1 is highly reproducible in the nonhuman primate (NHP) brain (Table 1). The coefficient of variation (CV) of the test and the retest PET scans was 10.7 and 12.0%, respectively, which further confirmed the small variability among different animals.

MicroPET Study of [^{11}C]CS1P1 in the Rat Brain and Spinal Cord.

A MicroPET imaging study of [^{11}C]CS1P1 in the normal rat brain and spinal cord was also performed. [^{11}C]CS1P1 entered the rat brain and spinal cord with a high uptake that was retained in the brain and spinal cord very well from 0 to 60 min post injection (Figure S3). The tracer uptake was high in the brain and cervical regions of the spinal cord, whereas the sacral region of the spinal cord showed the lowest uptake (Figure S3A). Within the brain, the tracer uptake was relatively high in the cortex, cerebellum, and thalamus, which is consistent with the *in vitro* autoradiography and immunostaining results (Figure S3B).

Radiometabolite Analysis of the NHP and Rat Plasma and Rat Brain Tissue Sample.

To further evaluate the *in vivo* stability of [^{11}C]CS1P1, radioactive metabolite analysis was performed for the NHP plasma samples post injection of [^{11}C]CS1P1 (Figure 5A). High-performance liquid chromatography (HPLC) metabolite analysis showed one major radioactive peak, the radioactive parent compound [^{11}C]CS1P1, and a negligible radioactive hydrophilic peak. The percentage of the remaining radioactive parent compound

[^{11}C]CS1P1 was 91, 92, and 90% at 5, 10, and 20 min post injection respectively, indicating that [^{11}C]CS1P1 has good *in vivo* stability.

Radiometabolite analysis was also performed in rats. For the rat plasma, HPLC metabolite analysis showed one major radioactive peak as in NHP plasma along with a minor radioactive hydrophilic peak. The radioactive metabolite was about 13.3 and 5.8% of total activity at 5 and 30 min, respectively (Figure 5B). To further explore whether the radioactive metabolite could cross the blood–brain barrier (BBB) and interfere with PET measures in the brain, HPLC metabolite analysis was performed with rat brain tissue homogenate samples post injection of [^{11}C]CS1P1. Only one major radioactive peak (the radioactive parent compound) was identified for the rat brain tissue homogenate sample. The amount of other radioactivity was negligible (Figure 5B), confirming that no radiometabolite entered into the brain, thus would not impact the PET measurement in the brain post injection of [^{11}C]CS1P1.

Kinetic Modeling.

Radiometabolite analysis indicated that [^{11}C]CS1P1 has high stability *in vivo*, and it is able to retain >90% of the parent compound at 20 min post injection. The blood radioactivity curve was fitted to a three-exponential model and is shown along with the metabolite-corrected plasma input function (mcPIF) in Figure 5C. Statistical analysis suggested that a two-compartment tissue model was optimal in fitting the model to the PET data. The model fit for the whole brain is shown in Figure 5C and for the various brain regions in Figure 5E,F.

DISCUSSION

The S1P-S1PR1 pathway has been implicated as a crucial mediator of many physiological and pathophysiological processes.[15–18] While most previous studies focused on studying the therapeutic effect of S1PR1 potent compounds, our group has reported a few S1PR1-specific radioligands for different inflammation models of diseases including MS, vascular injury, carotid injury, atherosclerosis, and LPS-induced inflammation in the liver.[14,19–21] To further characterize the potency and specificity of CS1P1 to S1PR1, we performed a saturation and competition binding assays. Saturation competitive binding assay indicated that CS1P1 is very potent to hS1PR1 as expected. To check the binding specificity *in vitro*, we used the endogenous S1PR ligand S1P, as well as two well-known S1PR agonists, SEW2871 and FTY720(S)-P, to compete with [^{3}H]CS1P1 binding with S1PR1. The S1P and FTY720(S)-P can displace CS1P1 with K_i values less than 10 nM, respectively, and SEW2871 showed a relatively low binding potency with S1PR1 with a K_i value of 354 nM, possibly because CS1P1 and SEW2871 binds to different sites of S1PR1 and therefore can only compete partially for [3H]CS1P1 binding with S1PR1 under our experimental conditions.

To further understand the role of S1PR1 and to characterize our S1PR1-specific radiotracer [^{11}C]CS1P1 in the CNS, we performed a comprehensive characterization of S1PR1 and its radioactive ligands, [^{3}H]CS1P1 and [^{11}C]CS1P1, in the human and NHP brain, as well as in the rat brain and spinal cord. Our study showed that S1PR1 is mainly expressed in the gray matter and with very low density in the white matter throughout the CNS for both humans

and rats. In the postmortem tissue of human brains, the relatively high radioactivity of [^{3}H]CS1P1 in several different regions of gray matter was almost 2-fold higher than that in the white matter. Among different gray matter regions, the thalamus, midbrain, and striatum showed a slightly higher radioactivity of [^{3}H]CS1P1 than the frontal cortex and cerebellum. Within the rat brain, the cortex, hippocampus, and hypothalamus showed the highest density of S1PR1, whereas corpus callosum showed the lowest density of S1PR1. The level of S1PR1 in the gray matter of the cerebellar cortex was about 4-fold higher than that in the cerebellum white matter. The microPET study in living animals also showed a similar pattern of [^{11}C]CS1P1 distribution in different regions of the brain. The higher amount of [^{11}C]CS1P1 in gray matter compared to white matter is of interest in MS, where gray matter atrophy is associated with disease progression.[22] Notably, the drug fingolimod, a functional antagonist of S1PR1, 3, 4, and 5, reduced brain atrophy in MS patients, particularly in deep gray matter structures.[23] Interestingly, PET showed a high uptake of [^{11}C]CS1P1 in the rat brain and cervical regions of the spinal cord, whereas the sacral region showed the lowest uptake of [^{11}C]CS1P1.

S1PRs are distributed throughout the CNS including endothelial cells at the BBB,[24] glial cells,[18,25] neural progenitor cells,[18] and oligodendrocytes.[26] While S1PR1 has been found to affect different physiological processes in the CNS such as regulation of neurotrophic gene,[27] control of energy homeostasis,[9] and regulation of the endothelial barrier,[28] advancing the understanding for the function and distribution of S1PR1 in the CNS is of crucial importance. Our study along with other previous studies[29–32] demonstrate that S1PR1 is preferentially distributed in the gray matter region of CNS. Furthermore, our findings using *in vitro* autoradiography, immunohistochemistry, and microPET studies also provide a detailed characterization of activated S1PR1 in postmortem human brain tissues and live animals including macaque and rat.

Compared with previous S1PR1 histological observations in the human brain,[29] our study also included rat brain and spinal cord. More importantly, we also performed an autoradiograph study using the [^{3}H]CS1P1 which shares the exact same molecular structure with [^{11}C]CS1P1 but radiolabeled with a different isotope. Our *in vitro* autoradiography study using [^{3}H]CS1P1 is able to quantitatively determine pharmacological binding parameters such as K_d and B_{max}.[33,34] Moreover, compared with the traditional immunohistochemical study that can only provide the distribution of antigen of interest, the autoradiography study provides both anatomical and functional information of S1PR1. Compared to other functional autoradiography analysis using GTP analogue guanosine-5′-*O*-(3-[^{35}S]thio)triphosphate ([^{35}S]GTPγS) combined with S1P or S1PR1-specific agonist SEW2871,[30–32] our study provides a direct distribution of activated S1PR1. Notably, both binding assays that used recombinant human S1PR1 membrane and autoradiograph study that used human and rat brain tissues showed the high binding potency and specificity of [^{3}H]CS1P1 to S1PR1 with K_d and K_i values of <10 nM. In addition, the B_{max}/K_d ratio, or binding potential (BP), measured using the saturation autoradiograph method was high in both human and rat brain tissues. BP reflects the capacity of a region of tissue for a ligand–receptor interaction, and most imaging agents targeting on receptor proteins in CNS have a BP ≥ 10, which is necessary for *in vivo* imaging on binding sites.[35]

Moreover, we also performed *in vivo* PET studies of [^{11}C]CS1P1 in the NHP brain, rat brain, and rat spinal cord. Although *in vitro* autoradiography and immunostaining have the advantage of visualizing spatial anatomy and even subcellular expression patterns, an *in vivo* PET study provides direct quantification of S1PR1 expression in living animals and therefore is more clinically relevant. Our microPET brain study in NHP showed that the tracer uptake was high in the striatum, prefrontal cortex, and the thalamus and low in the medial temporal lobe and cortical white matter. Our microPET study in rat showed that the uptake of [^{11}C]CS1P1 was high in the striatum, cortex, hippocampus, and hypothalamus but low in the white matter regions such as corpus callosum. Despite the different uptake of [^{11}C]CS1P1 in different brain regions, the microPET imaging data matched well with *in vitro* autoradiography and immunostaining results.

Our effort reported in this manuscript provided additional evidence to support that [^{11}C]CS1P1 is a promising S1PR1-specific radiotracer and suitable for PET imaging of CNS in living animals. Our microPET brain study in NHP showed that [^{11}C]CS1P1 had a high uptake in the majority of brain regions with a relatively small variance (% CV = 10.7). The TRV is small at 0.23%, indicating that the PET measurement of [^{11}C]CS1P1 in the NHP brain is highly reproducible. Our PET studies with [^{11}C]CS1P1 in the rat brain and spinal cord showed that [^{11}C]CS1P1 has relatively high uptake in the brain and upper region of the spinal cord, and the tracer distribution results matched well with results from immunostaining and autoradiography study. Furthermore, we have also performed the metabolite analysis of [^{11}C]CS1P1 in two species, the macaque and rat. Our radiometabolites analysis indicated that [^{11}C]CS1P1 has good *in vivo* stability for both macaque and rat. The parent radiotracer [^{11}C]CS1P1 is still >90% at 20 min in the macaque and rat plasma. The radiometabolite is negligible in macaque plasma samples, however, [^{11}C]CS1P1 in SD rat has a small amount of radiometabolite identified at 5 min post injection, and this small amount of radiometabolite was not detectable at 30 min, suggesting that the metabolism of [^{11}C]CS1P1 has species difference and is faster in SD rat than that in macaque. Nevertheless, no radiometabolite was identified in the SD rat brain homogenate, suggesting that radioactive metabolites do not penetrate the BBB or accumulate in the brain post injection of [^{11}C]CS1P1.

In conclusion, we performed detailed characterizations of a tritiated S1PR1-specific radioligand [^{3}H]CS1P1 using human postmortem brain tissues, rat brain tissues, and spinal cord. Our immunohistochemistry studies with S1PR1-specific antibody for adjacent tissue slides confirmed the distribution of [^{3}H]CS1P1 in autoradiography. Our autoradiography and immunostaining study results provide a detailed distribution of S1PR1 particular functional S1PR1 in the human brain, as well as rat brain and spinal cord, which may offer a better understanding of the role of S1PR1 in CNS. Our PET imaging studies in both cynomolgus macaques and rats also demonstrated that [^{11}C]CS1P1 is a highly potent and specific radiotracer for S1PR1 with good test–retest reliability and very small variability among different animals, and the distribution of [^{11}C]CS1P1 in brain regions was consistent with autoradiography results using [^{3}H]CS1P1 and immunostaining using S1PR1-specific antibody. Our HPLC radiometabolite analysis of the NHP and rat plasma samples and the rat brain homogenate suggests that [^{11}C]CS1P1 has very good *in vivo* stability, and no radioactive metabolite can enter into the brain to interfere with the PET measurement

of S1P1 expression in the brain. Overall, this study further suggests that [^{11}C]CS1P1 is a suitable PET radioligand for investigating S1PR1 function in CNS. We expect that our ongoing clinical studies in human subjects will demonstrate the suitability of [^{11}C]CS1P1 as a S1PR1 radiotracer for clinical use.

MATERIALS AND METHODS

Human Brain Tissues.

Human brain tissues were obtained from the Charles F. and Joanne Knight Alzheimer Disease Research Center at the Washington University in St Louis and the Rocky Mountain Multiple Sclerosis Center Tissue Bank at the University of Colorado and used in accordance with Washington University guidelines of using postmortem tissues. All samples were snap-frozen and stored at −80 °C until used.

Animals.

All animal experiments were conducted by following the Guidelines for the Care and Use of Research Animals under a research protocol approved by the Washington University Institutional Animal Care and Use Committee (IACUC). The NHP study was conducted in the NHP microPET facility at the Washington University School of Medicine in St. Louis. Six adult male cynomolgus macaques (*Macaca fascicularis*) (8–10 kg) were used in this study. Animals were prepared for microPET studies, as previously reported.[21] Each animal was initially anesthetized with ketamine (10–20 mg/kg) and injected with glycopyrrolate (0.013–0.017 mg/kg) to reduce saliva secretions. 40% N_2O and 60% O_2 with 1.0–1.5% isoflurane inhalation anesthesia was maintained throughout the microPET imaging sessions. A 20-gauge plastic catheter was inserted into a limb vein to permit hydration and injection of the radiotracer. Arterial blood was collected through another 20-gauge plastic catheter which was placed into a femoral artery. Wild-type Sprague Dawley (Charles River, Wilmington, MA) was used, and the entire rat study was conducted in Preclinical Imaging Facility at the Washington University School of Medicine in St. Louis. Rats were prepared for microPET studies, as previously reported.[14]

Radioligand Preparation.

[^{3}H]CS1P1 (Figure 1A) was custom synthesized by NOVANDI Chemistry AB (Sweden) using our homemade precursors, from our laboratory, at a specific activity of 2997 GBq/mmol. [^{11}C]CS1P1 (Figure 1A) was produced in our radiochemistry facility, as previously described.[12] The radiosynthesis of [^{11}C]CS1P1 was accomplished with a radiochemical purity of >99%, chemical purity of >95%, and molar activity from 48 to 93 GBq/μmol (decay-corrected to the end of synthesis). [^{3}H]CS1P1 and [^{11}C]CS1P1 share exactly the same chemical structure except labeled with different isotopes.

Saturation Binding Assay.

Saturation binding assay was carried out using [^{3}H]CS1P1. In brief, 2 μg of S1PR1 membrane protein (Millipore, Billerica, MA) was incubated with a serial dilution of [^{3}H]CS1P1 ranging from 1 to 32 nM in 150 μL of 50 mM HEPES (pH 7.5), 5 mM $MgCl_2$, 1 mM $CaCl_2$, and 0.5% fatty acid-free bovine serum albumin (BSA) in a 96-well

polypropylene plate (Fisher Scientific, Pittsburgh, PA) for 1 h with gentle shaking at room temperature. Samples were filtered and washed three times using a presoaked 96-well glass fiber filtration plate (Millipore, Billerica, MA). The filter was then transferred to a scintillation vial with 2 mL of scintillation fluid and counted on a Beta liquid scintillation counter. Non-specific binding was determined by adding 10 μM cold CS1P1.

Competition Binding Assay.

Competition binding assay was carried out similarly as saturation binding assay using [^{3}H]CS1P1 competing with S1P (Sigma-Aldrich, St Louis, MO), SEW2871 (Tocris, Bristol, UK), and FTY720(S)-P (Cayman, Ann Arbor, MI). S1P is the endogenous ligand to S1PR, whereas SEW2871[31,36] and FTY720(S)-P[37] are well-known potent S1PR agonists. In brief, 2 μg of the S1PR1 membrane was incubated with 8 nM [^{3}H]CS1P1 and a serial dilution of candidate compounds ranging from 0.1 nM to 10 μM. The membrane was then filtered, washed, and counted, as described above.

Autoradiography Study in the Human Brain, Rat Brain, and Spinal Cord.

In vitro autoradiography study was carried out using [^{3}H]CS1P1 in frozen sections from various regions of postmortem human brain tissues, as well as from adult SD rat brains and spinal cords. In brief, 14 μm sections were pre-incubated with HBSS buffer containing 10 mM HEPES, 5 mM $MgCl_2$, 0.2% BSA, and 0.1 mM EDTA at pH 7.4 for 5 min at room temperature (RT). The sections were then incubated with 0.5 nM [^{3}H]CS1P1 in buffer for 1 h at RT with gentle shaking, washed with buffer for 5 min at RT for three times, and then dipped in ice-cold H_2O for 1 min and air dried overnight. Dried slides were incubated with the Carestream BioMax autoradiography film (Carestream, Rochester, NY) in a Hypercassette autoradiography cassette (Cytiva, Amersham, UK) for 15 days along with an ART-123 Tritium Standards (American Radiolabeled Chemicals, St Louis, MO). The film was then processed using a Kodak film developer (Kodak, Rochester, NY). To determine the non-specific binding, 10 μM of S1PR1-specific antagonist, NIBR-0213 (Cayman, Ann Arbor, MI), was used. All images were processed and analyzed using Fiji ImageJ,[38] and all representative images showed were processed using a continuous lut “Physics.” Brain regions were selected from the autoradiographic images according to the hematoxylin staining in the adjacent slide. Regions of interest (ROIs) were randomly selected in the different regions of the brain, and the intensity was measured. The intensity from specific binding was accessed by subtracting the intensity in non-specific binding from the total binding.

For the saturation autoradiography study, sections were incubated, washed, and developed, as described above with a serial dilution of [^{3}H]CS1P1 ranging from 0.5 to 16 nM. 14 micron sections were pre-incubated with HBSS buffer containing 10 mM HEPES, 5 mM $MgCl_2$, 0.2% BSA, and 0.1 mM EDTA at pH7.4 for 5 min at RT. Sections were then incubated with a serial dilution including 0.5, 1, 2, 4, 8, and 16 nM of [^{3}H]CS1P1 in buffer for 1 h at RT, then washed, and air dried overnight. Dried slides were incubated with the BioMax autoradiography film for 15 days along with an ART-123 Tritium Standards and processed using a Kodak film developer. The non-specific binding blocking was determined by incubation in the presence of 10 μM NIBR-0213.

Immunohistochemical Staining.

Immunohistochemical staining of S1PR1 was carried out in frozen sections from various regions of postmortem human brain tissues, as well as from adult SD rat brains and spinal cords using anti-S1PR1 polyclonal antibody (Alomone, Jerusalem, Israel). In brief, 14 μm sections were fixed in 4% paraformaldehyde and then blocked with BLOXALL Blocking Solution (Vector Laboratories, Burlingame, CA). Antigen retrieval was performed by incubating sections with Antigen Unmasking Solution (Vector Laboratories, Burlingame, CA) in a steamer for 30 min. After blocking with 5% horse serum for 1 h at RT, all sections were stained using anti-S1PR1 antibody at 4 °C overnight followed by washing and incubating with the ImmPRESS HRP Horse anti-rabbit polymer and then developed using ImmPACT DAB (Vector Laboratories, Burlingame, CA). Mounted sections were scanned using the NanoZoomer system (Hamamatsu, Japan).

MicroPET Studies in the Brains of Cynomolgus Macaques.

The microPET study was carried out using a microPET Focus-220 scanner (Siemens Microsystems, Knoxville, TN), as described previously.[21] Prior to each PET emission acquisition, a 45 min transmission scan for attenuation correction was performed following a 10 min transmission that was used to check the position of the brain within the scanner. After administration of ~0.3–0.4 GBq [with molar activity from 48 to 93 GBq/μmol (EOB)] of a radiotracer, 2 h dynamic emission scan data were acquired using the following time frames: 3 × 1 min, 4 × 2 min, 3 × 3 min, and 20 × 5 min. A filtered back projection method was used to reconstruct PET images (volume size: 12 × 128 × 95, voxel size: 1.898 × 1.898 × 0.796 mm^3 in the *x, y,* and *z* direction) with dead time, scatter, randomes, and attenuation correction. The reconstructed PET image has a spatial resolution of 2.4 mm full-width at half maximum in all three dimensions at the center of the field of view. To quantify the total tracer uptake in the brain and the tracer uptake in subregions of the brain, dynamic PET images were co-registered to a standardized monkey MRI template[39] using automated image registration program “Fuse It” in PMOD software 4.02 (PMOD technologies, Zürich, Switzerland). Predefined brain ROIs from the template including prefrontal, basal frontal, and anterior cingulate cortex, caudate and putamen, insula, lateral and medial temporal lobes, amygdala, hippocampus, thalamus, hypothalamus, parietal lobe, posterior cingulate cortex, occipital lobe, pons, mid brain, corpus callosum, cortical white matter, and cerebellum were applied to the co-registered PET image to obtain the regional time–activity curves (TACs). The uptake of radioactivity was normalized to body weight and the dose of radioactivity injected to obtain SUV. TRV in a total of six NHPs under baseline conditions was conducted.

MicroPET Studies for the SD Rat Brain and Spinal Cord.

MicroPET studies in rats were carried out using an Inveon PET/CT system (Siemens Inc., Knoxville, TN) by following previous procedures.[14] Following a CT scan, a 60 min dynamic emission scan was acquired with the flowing time frames: 1 × 3, 6 × 2, 9 × 5, 6 × 10, 4 × 30, 2 × 60 s, 2 × 2, and 10 × 5 min after administration of ~18.5 MBq of the radiotracer. The reconstructed PET image was analyzed using Inveon Research Workstation software IRW 4.2 (Siemens Inc., Knoxville, TN). ROIs including brain and cervical, thoracic, lumbar, and

sacral segments of spinal cord were drawn over the co-registered PET/CT images. The SUV was calculated by normalizing with body weight and injection dose.

Radiometabolite Studies of Macaque Plasma Samples.

The radiometabolite study in NHP plasma was performed according to the previous procedure.[40] Arterial blood samples (1.2–1.5 mL) were collected in a heparinized syringe at 5, 10, and 20 min post-injection. Plasma (400 μL) was collected by centrifugation of the whole blood and mixed with ice-cold acetonitrile (1.2 mL) to deproteinate and extract the parent compound and radiolabeled metabolites. After centrifugation, the supernatant (200 μL) was loaded onto an analytical HPLC system composed of an Agilent SB C-18 analytical HPLC column (250 mm × 4.6 mm, 5 μm) and a UV detector with 254 nm wavelength. The mobile phase was acetonitrile/0.1 M ammonium formate buffer (pH 4.5) (75/25, v/v) with a flow rate of 1.13 mL/min. The eluted fractions were collected at 1 min interval, and total 15 samples from 0 to 16 min were collected; upon the completion of the 15 sample fraction collection for each HPLC sample injection, a gamma counter was used to measure the radioactivity of each 1 min fraction sample collection. After decay correction of each sample's radioactivity, chromatograph of each sample on the HPLC was rebuilt.

Radiometabolite Study of the Rat Plasma and Brain Homogenate.

To confirm whether any radioactive metabolite entered into the brain, the radioactive metabolite study was also carried out using rat plasma and brain homogenate samples post injection of the radiotracer into the rat. Adult male SD rats were intravenously injected with ~37 MBq of [^{11}C]CS1P1 and were sacrificed at 5 and 30 min. Blood samples were collected directly from the left ventricle in a heparinized syringe. Brains were dissected and manually homogenized in cold PBS buffer with a Teflon homogenizer. 1 mL of whole blood or brain homogenate was further processed following the similar procedure of preparing the NHP blood samples.

Whole Blood and Plasma Collection for the Arterial Blood Input Function.

Arterial blood samples from NHP were collected from the femoral artery post-injection of [^{11}C]CS1P1. Sequential discrete arterial blood samples were collected in heparinized syringes for approximately at every 10 s for a total of 15 samples, then every 15 s for a total of 10 samples, and then every 1 min for a total eight samples, and every 5 min for a total of six samples, and every 15 min for a total of four samples, and the last sample at the end of 2 h's scan. Whole blood samples were counted on a Beckman 8000 automated gamma counter (Beckman, Brea, CA) and then centrifuged; the plasma samples were collected and counted on the Beckman 8000 automated gamma counter. The activity was then calculated as background and decay-corrected. The percentile of unmetabolized [^{11}C]CS1P1 was determined from the radioactive metabolite study.

PET Imaging Modeling.

Total blood and plasma TACs were optimized against a mixed three-compartmental Gaussian model. The plasma TAC was corrected for metabolites to generate the mcPIF. The mcPIF and blood activity curves were used to optimize two-tissue compartmental models

against total brain and specific brain region TACs with a parameter to account for the vascular fraction. Pseudo-Poisson weighting was used in optimizing the model against PET data. Kinetic modeling was performed using the kinetics module in PMOD ver 4.02.

Statistical Analysis.

All data were analyzed with Prism 7.0 (GraphPad Software, San Diego, CA). For binding data and autoradiography data, the equilibrium dissociation constant (K_d) and maximum number of binding sites (B_{max}) were determined by nonlinear regression analysis of one site saturation or competitive binding model using Prism. To determine the test–retest reliability of the PET brain studies of [^{11}C]CS1P1 in NHP, percentage TRV was calculated as the mean percentage between the absolute difference in test and retest and average test and retest values using the equation as

$$100 \times |\text{SUV-test} - \text{SUV-retest}| / ((\text{SUV-test} + \text{SUV-retest})/2)$$

The CV (CV = 100 × standard deviation/mean SUV) is a measure of dispersion and is often referred to as the relative standard deviation.

Supplementary Material

Refer to Web version on PubMed Central for supplementary material.

ACKNOWLEDGMENTS

We would like to acknowledge the Rocky Mountain Multiple Sclerosis Center Tissue Bank for kindly providing postmortem human brain tissues. We would like to acknowledge Robert Dennett and Michael Nickels at the Washington University Cyclotron Facility. We especially would like to acknowledge Lynne Jones, Emily Williams, Emily Flores, and John Hood for their technical assistance and helpful discussions. We also would like to acknowledge Nicole Fettig and Lori Strong at the Mallinckrodt Institute of Radiology Preclinical Imaging Facility for their technical assistance.

Funding

This work is supported by the National Institutes of Health under projects NS075527, NS103957, NS103988, and EB025815.

REFERENCES

(1). Lee O-H; Kim Y-M; Lee YM; Moon E-J; Lee D-J; Kim J-H; Kim K-W; Kwon Y-G Sphingosine 1-phosphate induces angiogenesis: its angiogenic action and signaling mechanism in human umbilical vein endothelial cells. Biochem. Biophys. Res. Commun 1999, 264, 743–750. [PubMed: 10544002]

(2). Wang G; Bieberich E Sphingolipids in neurodegeneration (with focus on ceramide and S1P). Adv. Biol. Regul 2018, 70, 51–64. [PubMed: 30287225]

(3). Chi H Sphingosine-1-phosphate and immune regulation: trafficking and beyond. Trends Pharmacol. Sci 2011, 32, 16–24. [PubMed: 21159389]

(4). Brinkmann V; Davis MD; Heise CE; Albert R; Cottens S; Hof R; Bruns C; Prieschl E; Baumruker T; Hiestand P; Foster CA; Zollinger M; Lynch KR The immune modulator FTY720 targets sphingosine 1-phosphate receptors. J. Biol. Chem 2002, 277, 21453–21457. [PubMed: 11967257]

(5). Brinkmann V; Billich A; Baumruker T; Heining P; Schmouder R; Francis G; Aradhye S; Burtin P Fingolimod (FTY720): discovery and development of an oral drug to treat multiple sclerosis. Nat. Rev. Drug Discovery 2010, 9, 883–897. [PubMed: 21031003]

(6). Blaho VA; Hla T An update on the biology of sphingosine 1-phosphate receptors. J. Lipid Res 2014, 55, 1596–1608. [PubMed: 24459205]

(7). Ye Y; Zhao Z; Xu H; Zhang X; Su X; Yang Y; Yu X; He X Activation of Sphingosine 1-Phosphate Receptor 1 Enhances Hippocampus Neurogenesis in a Rat Model of Traumatic Brain Injury: An Involvement of MEK/Erk Signaling Pathway. Neural Plast 2016, 2016, 8072156. [PubMed: 28018679]

(8). Chen Z; Doyle TM; Luongo L; Largent-Milnes TM; Giancotti LA; Kolar G; Squillace S; Boccella S; Walker JK; Pendleton A; Spiegel S; Neumann WL; Vanderah TW; Salvemini D Sphingosine-1-phosphate receptor 1 activation in astrocytes contributes to neuropathic pain. Proc. Natl. Acad. Sci 2019, 116, 10557–10562. [PubMed: 31068460]

(9). Silva VRR; Katashima CK; Bueno Silva CG; Lenhare L; Micheletti TO; Camargo RL; Ghezzi AC; Camargo JA; Assis AM; Tobar N; Morari J; Razolli DS; Moura LP; Pauli JR; Cintra DE; Velloso LA; Saad MJA; Ropelle ER Hypothalamic S1P/S1PR1 axis controls energy homeostasis in Middle-Aged Rodents: the reversal effects of physical exercise. Aging 2016, 9, 142–155. [PubMed: 28039439]

(10). Van Doorn R; Van Horssen J; Verzijl D; Witte M; Ronken E; Van Het Hof B; Lakeman K; Dijkstra CD; Van Der Valk P; Reijerkerk A; Alewijnse AE; Peters SLM; De Vries HE Sphingosine 1-phosphate receptor 1 and 3 are upregulated in multiple sclerosis lesions. Glia 2010, 58, 1465–1476. [PubMed: 20648639]

(11). Tsai H-C; Nguyen K; Hashemi E; Engleman E; Hla T; Han MH Myeloid sphingosine-1-phosphate receptor 1 is important for CNS autoimmunity and neuroinflammation. J. Autoimmun 2019, 105, 102290. [PubMed: 31202617]

(12). Jin H; Yang H; Liu H; Zhang Y; Zhang X; Rosenberg AJ; Liu Y; Lapi SE; Tu Z A promising carbon-11-labeled sphingosine-1-phosphate receptor 1-specific PET tracer for imaging vascular injury. J. Nucl. Cardiol 2017, 24, 558–570. [PubMed: 26843200]

(13). Liu H; Jin H; Han J; Yue X; Yang H; Zayed MA; Gropler RJ; Tu Z Upregulated Sphingosine 1-Phosphate Receptor 1 Expression in Human and Murine Atherosclerotic Plaques. Mol. Imaging Biol 2018, 20, 448–456. [PubMed: 29134505]

(14). Liu H; Jin H; Yue X; Luo Z; Liu C; Rosenberg AJ; Tu Z PET Imaging Study of S1PR1 Expression in a Rat Model of Multiple Sclerosis. Mol. Imaging Biol 2016, 18, 724–732. [PubMed: 26975859]

(15). Kim HJ; Miron VE; Dukala D; Proia RL; Ludwin SK; Traka M; Antel JP; Soliven B Neurobiological effects of sphingosine 1-phosphate receptor modulation in the cuprizone model. FASEB J 2011, 25, 1509–1518. [PubMed: 21248243]

(16). Choi JW; Chun J Lysophospholipids and their receptors in the central nervous system. Biochim. Biophys. Acta 2013, 1831, 20–32. [PubMed: 22884303]

(17). Cuzzocrea S; Doyle T; Campolo M; Paterniti I; Esposito E; Farr SA; Salvemini D Sphingosine 1-Phosphate Receptor Subtype 1 as a Therapeutic Target for Brain Trauma. J. Neurotrauma 2018, 35, 1452–1466. [PubMed: 29310513]

(18). Kimura A; Ohmori T; Ohkawa R; Madoiwa S; Mimuro J; Murakami T; Kobayashi E; Hoshino Y; Yatomi Y; Sakata Y Essential Roles of Sphingosine 1-Phosphate/S1P1Receptor Axis in the Migration of Neural Stem Cells Toward a Site of Spinal Cord Injury. Stem Cells 2007, 25, 115–124. [PubMed: 16990586]

(19). Rosenberg AJ; Liu H; Jin H; Yue X; Riley S; Brown SJ; Tu Z Design, Synthesis, and In Vitro and In Vivo Evaluation of an ^{18}F-Labeled Sphingosine 1-Phosphate Receptor 1 (S1P1) PET Tracer. J. Med. Chem 2016, 59, 6201–6220. [PubMed: 27280499]

(20). Luo Z; Rosenberg AJ; Liu H; Han J; Tu Z Syntheses and in vitro evaluation of new S1PR1 compounds and initial evaluation of a lead F-18 radiotracer in rodents. Eur. J. Med. Chem 2018, 150, 796–808. [PubMed: 29604582]

(21). Luo Z; Han J; Liu H; Rosenberg AJ; Chen DL; Gropler RJ; Perlmutter JS; Tu Z Syntheses and in vitro biological evaluation of S1PR1 ligands and PET studies of four F-18 labeled radiotracers in the brain of nonhuman primates. Org. Biomol. Chem 2018, 16, 9171–9184. [PubMed: 30462126]

(22). Zivadinov R; Bergsland N; Dolezal O; Hussein S; Seidl Z; Dwyer MG; Vaneckova M; Krasensky J; Potts JA; Kalincik T; Havrdová E; Horáková D Evolution of cortical and thalamus atrophy and disability progression in early relapsing-remitting MS during 5 years. Am. J. Neuroradiol 2013, 34, 1931–1939. [PubMed: 23578679]

(23). Gaetano L; Häring DA; Radue E-W; Mueller-Lenke N; Thakur A; Tomic D; Kappos L; Sprenger T Fingolimod effect on gray matter, thalamus, and white matter in patients with multiple sclerosis. Neurology 2018, 90, e1324–e1332. [PubMed: 29540589]

(24). van Doorn R; Nijland PG; Dekker N; Witte ME; Lopes-Pinheiro MA; van het Hof B; Kooij G; Reijerkerk A; Dijkstra C; van van der Valk P; van Horssen J; de Vries HE Fingolimod attenuates ceramide-induced blood-brain barrier dysfunction in multiple sclerosis by targeting reactive astrocytes. Acta Neuropathol 2012, 124, 397–410. [PubMed: 22810490]

(25). Sorensen SD; Nicole O; Peavy RD; Montoya LM; Lee CJ; Murphy TJ; Traynelis SF; Hepler JR Common signaling pathways link activation of murine PAR-1, LPA, and S1P receptors to proliferation of astrocytes. Mol. Pharmacol 2003, 64, 1199–1209. [PubMed: 14573770]

(26). Jaillard C; Harrison S; Stankoff B; Aigrot MS; Calver AR; Duddy G; Walsh FS; Pangalos MN; Arimura N; Kaibuchi K; Zalc B; Lubetzki C Edg8/S1P5: an oligodendroglial receptor with dual function on process retraction and cell survival. J. Neurosci 2005, 25, 1459–1469. [PubMed: 15703400]

(27). Tran C; Heng B; Teo JD; Humphrey SJ; Qi Y; Couttas TA; Stefen H; Brettle M; Fath T; Guillemin GJ; Don AS Sphingosine 1-phosphate but not Fingolimod protects neurons against excitotoxic cell death by inducing neurotrophic gene expression in astrocytes. J. Neurochem 2020, 153, 173–188. [PubMed: 31742704]

(28). Anwar M; Mehta D Post-translational modifications of S1PR1 and endothelial barrier regulation. Biochim. Biophys. Acta, Mol. Cell Biol. Lipids 2020, 1865, 158760. [PubMed: 32585303]

(29). Nishimura H; Akiyama T; Irei I; Hamazaki S; Sadahira Y Cellular localization of sphingosine-1-phosphate receptor 1 expression in the human central nervous system. J. Histochem. Cytochem 2010, 58, 847–856. [PubMed: 20566754]

(30). Waeber C; Chiu ML In vitro autoradiographic visualization of guanosine-5′-O-(3-[35S]thio)triphosphate binding stimulated by sphingosine 1-phosphate and lysophosphatidic acid. J. Neurochem 1999, 73, 1212–1221. [PubMed: 10461914]

(31). Sanna MG; Liao J; Jo E; Alfonso C; Ahn M-Y; Peterson MS; Webb B; Lefebvre S; Chun J; Gray N; Rosen H Sphingosine 1-phosphate (S1P) receptor subtypes S1P1 and S1P3, respectively, regulate lymphocyte recirculation and heart rate. J. Biol. Chem 2004, 279, 13839–13848. [PubMed: 14732717]

(32). Sim-Selley LJ; Goforth PB; Mba MU; Macdonald TL; Lynch KR; Milstien S; Spiegel S; Satin LS; Welch SP; Selley DE Sphingosine-1-phosphate receptors mediate neuromodulatory functions in the CNS. J. Neurochem 2009, 110, 1191–1202. [PubMed: 19493165]

(33). Maguire JJ; Kuc RE; Davenport AP Radioligand binding assays and their analysis. Methods Mol. Biol 2012, 897, 31–77. [PubMed: 22674160]

(34). Dong C; Liu Z; Wang F Radioligand saturation binding for quantitative analysis of ligand-receptor interactions. Biophys. Rep 2015, 1, 148–155. [PubMed: 27471749]

(35). Patel S; Gibson R In vivo site-directed radiotracers: a mini-review. Nucl. Med. Biol 2008, 35, 805–815. [PubMed: 19026942]

(36). Hale JJ; Lynch CL; Neway W; Mills SG; Hajdu R; Keohane CA; Rosenbach MJ; Milligan JA; Shei G-J; Parent SA; Chrebet G; Bergstrom J; Card D; Ferrer M; Hodder P; Strulovici B; Rosen H; Mandala S A rational utilization of high-throughput screening affords selective, orally bioavailable 1-benzyl-3-carboxyazetidine sphingosine-1-phosphate-1 receptor agonists. J. Med. Chem 2004, 47, 6662–6665. [PubMed: 15615513]

(37). Valentine WJ; Kiss GN; Liu J; E S; Gotoh M; Murakami-Murofushi K; Pham TC; Baker DL; Parrill AL; Lu X; Sun C; Bittman R; Pyne NJ; Tigyi G (S)-FTY720-Vinylphosphonate, an analogue of the immunosuppressive agent FTY720, is a pan-antagonist of sphingosine 1-

phosphate GPCR signaling and inhibits autotaxin activity. Cell Signal 2010, 22, 1543–1553. [PubMed: 20566326]

(38). Schindelin J; Arganda-Carreras I; Frise E; Kaynig V; Longair M; Pietzsch T; Preibisch S; Rueden C; Saalfeld S; Schmid B; Tinevez J-Y; White DJ; Hartenstein V; Eliceiri K; Tomancak P; Cardona A Fiji: an open-source platform for biological-image analysis. Nat. Methods 2012, 9, 676–682. [PubMed: 22743772]

(39). Yasuno F; Brown AK; Zoghbi SS; Krushinski JH; Chernet E; Tauscher J; Schaus JM; Phebus LA; Chesterfield AK; Felder CC; Gladding RL; Hong J; Halldin C; Pike VW; Innis RB The PET radioligand [11C]MePPEP binds reversibly and with high specific signal to cannabinoid CB1 receptors in nonhuman primate brain. Neuropsychopharmacology 2008, 33, 259–269. [PubMed: 17392732]

(40). Tu Z; Zhang X; Jin H; Yue X; Padakanti PK; Yu L; Liu H; Flores HP; Kaneshige K; Parsons SM; Perlmutter JS Synthesis and biological characterization of a promising F-18 PET tracer for vesicular acetylcholine transporter. Bioorg. Med. Chem 2015, 23, 4699–4709. [PubMed: 26138195]

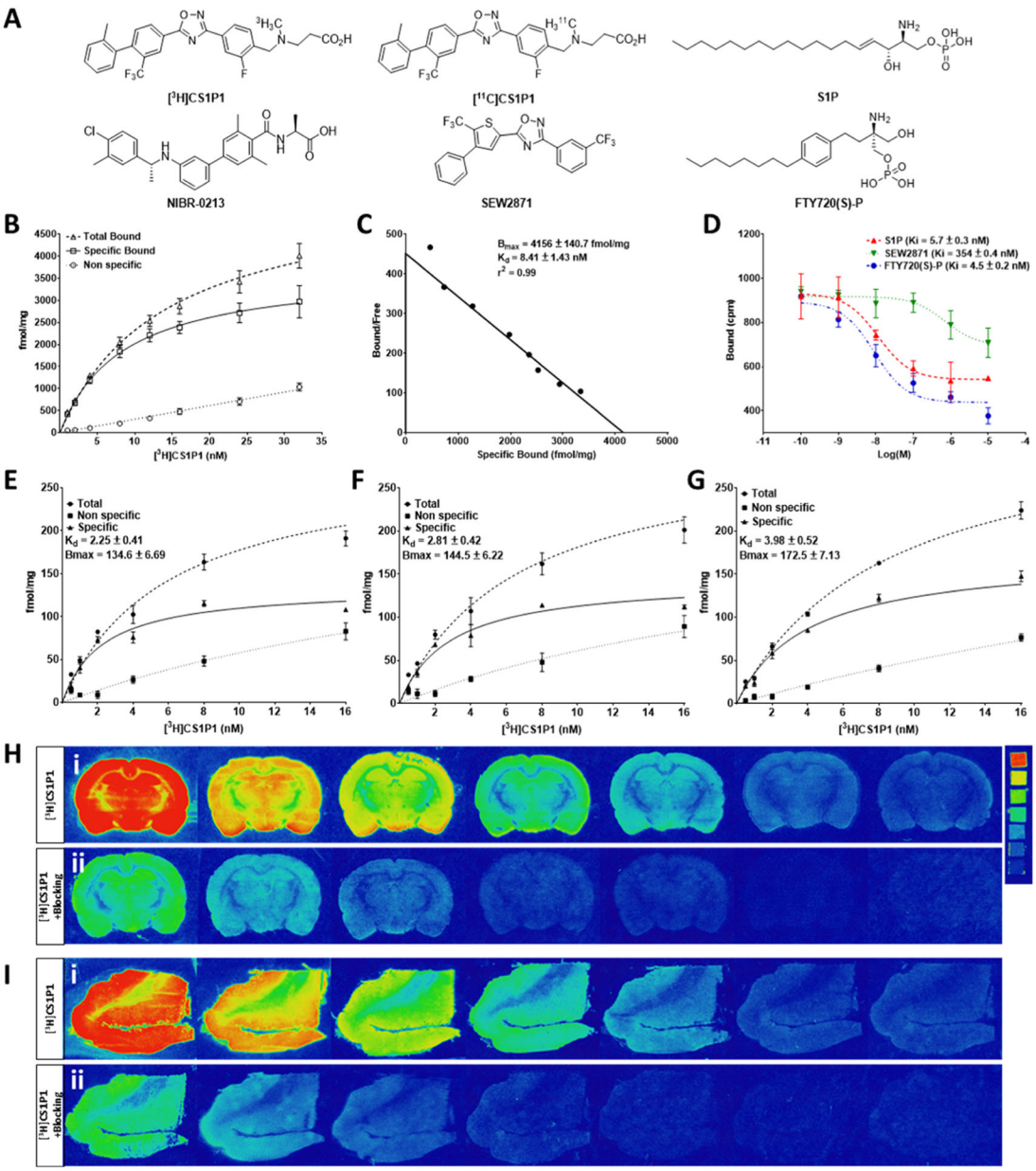

Figure 1.

In vitro characterization of potency and specificity of [^{3}H]CS1P1 toward S1PR1. (A) Chemical structures of CS1P1 and other compounds used in this study. (B–D) Saturation and competition binding assay of [^{3}H]CS1P1 with recombinant human S1PR1 membrane: saturation binding assay showed a high affinity of [^{3}H]CS1P1 to hS1PR1 with a K_d of 8.41 nM (B–C); [^{3}H]CS1P1 can compete with the known potent S1PR1 ligand and S1P with a K_i value of 5.7 nM for S1P, 4.5 nM for FTY720(S)-P, and 354 nM for SWE2871 (D). (E–I) Saturation binding autoradiograph analysis of [^{3}H]CS1P1 in the human and rat brain: (E) Saturation binding assay showed a high affinity of [^{3}H]CS1P1 to the gray matter of the human frontal cortex with a K_d of 8.54 nM; (F) saturation binding assay showed a high affinity of [^{3}H]CS1P1 to the cortex region of the rat brain with a K_d of 5.94 nM; (G)

saturation binding assay showed a high affinity of [^{3}H]CS1P1 to the hippocampus region of the rat brain with a K_d of 6.57 nM; (H) representative images of saturation binding autoradiograph analysis of [^{3}H]CS1P1 in the rat brain and image of tritium ART-123 standard (activities of standard from top to bottom in μC_i/g: 489.1, 243, 138.1, 63.1, 36.3, 16.6, and 8); (I) representative images of saturation binding autoradiograph analysis of [^{3}H]CS1P1 in the human frontal cortex.

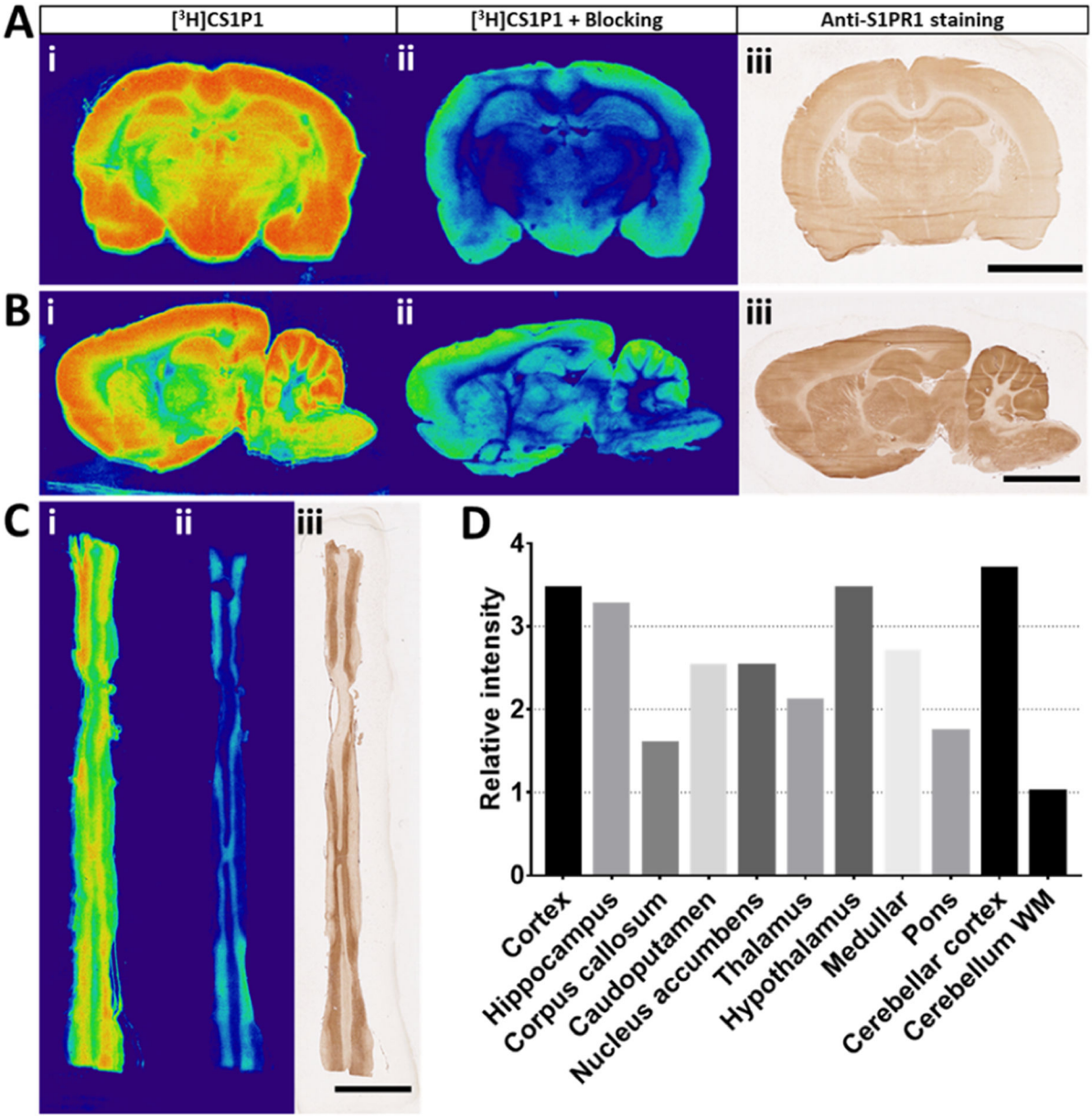

Figure 2.

In vitro characterization of [^{3}H]CS1P1 and S1PR1 in CNS of rat. (A–C) *In vitro* autoradiography of [^{3}H]CS1P1 and immunostaining of S1PR1 in the rat brain and spinal cord. [^{3}H]CS1P1 autoradiograph (i), autoradiograph with NIBR-0213 blocking (ii), and immunostaining (iii) were performed in the rat brain (A,B) and spinal cord (C). Autoradiograph study showed that [^{3}H]CS1P1 is mainly distributed in gray matter with no to very low amount in the white matter in both brain and spinal cord; [^{3}H]CS1P1 can be blocked by S1PR1-specific antagonist NIBR-0213; the distribution of [^{3}H]CS1P1 matched well with immunostaining with anti-S1PR1 (scale bar = 5 mm); (D) relative radioactivity of [^{3}H]CS1P1 in different regions of the rat brain: WM has a relatively low level of bound [^{3}H]CS1P1, whereas GM has a much higher level of bound [3H]CS1P1, among

all tested regions, cerebellum WM has the lowest level of bound [^{3}H]CS1P1, and cortex, hypothalamus, and cerebellar cortex show the highest level of bound [^{3}H]CS1P1. GM: gray matter, WM: white matter.

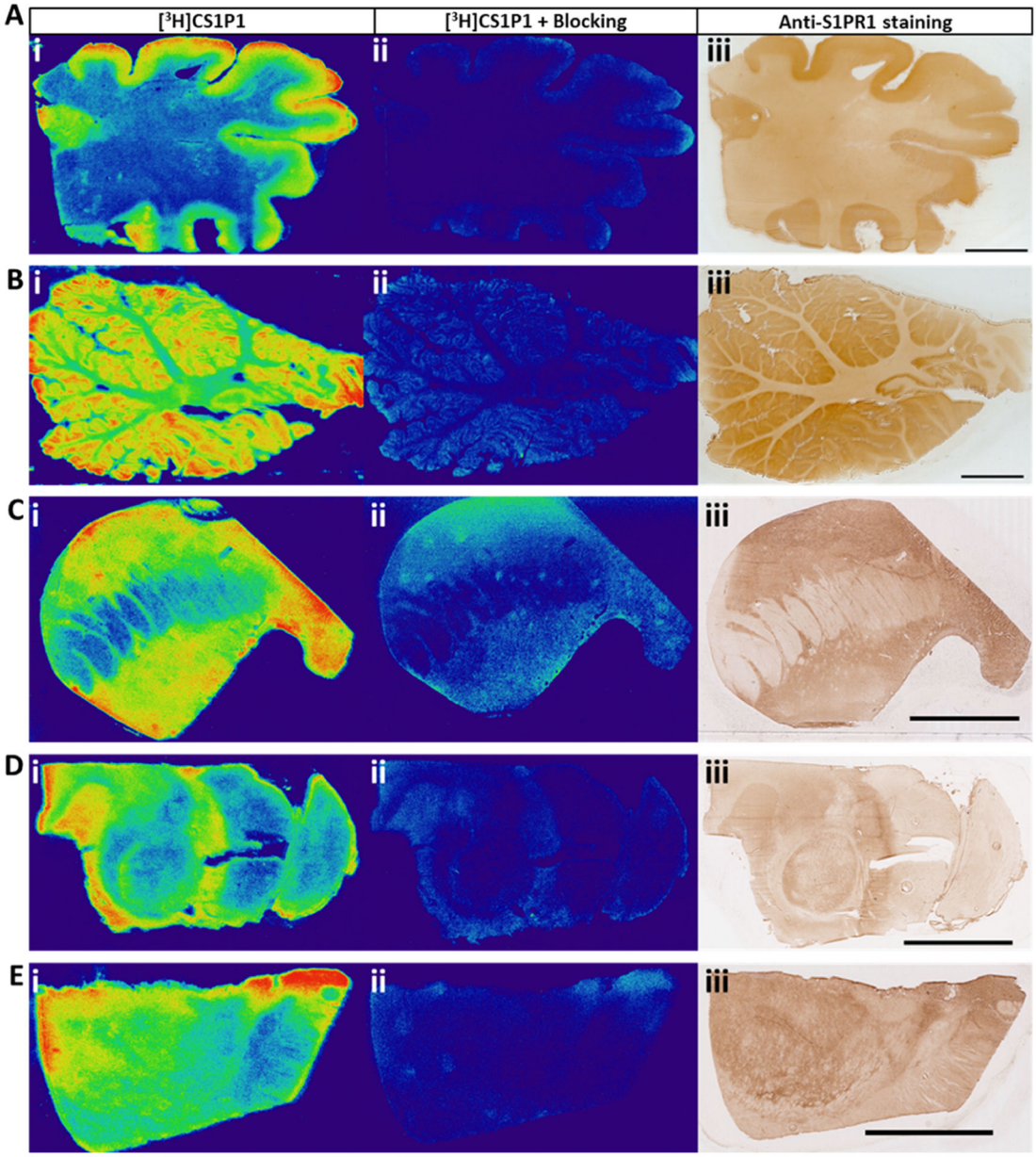

Figure 3.

In vitro autoradiography of [^{3}H]CS1P1 and immunostaining of S1PR1 in the human brain. (A–E) [^{3}H]CS1P1 autoradiograph (i), autoradiograph with NIBR-0213 blocking (ii), and immunostaining (iii) were performed in the human frontal cortex (A), cerebellum (B), striatum (C), midbrain (D), and thalamus (E). Autoradiograph study showed that [^{3}H]CS1P1 is mainly distributed in gray matter with no to very low amount in the white matter; [^{3}H]CS1P1 can be blocked by S1PR1-specific antagonist NIBR-0213; the distribution of [^{3}H]CS1P1 matched well with immunostaining with anti-S1PR1 (scale bar = 1 cm for A and B and 5 mm for C–E).

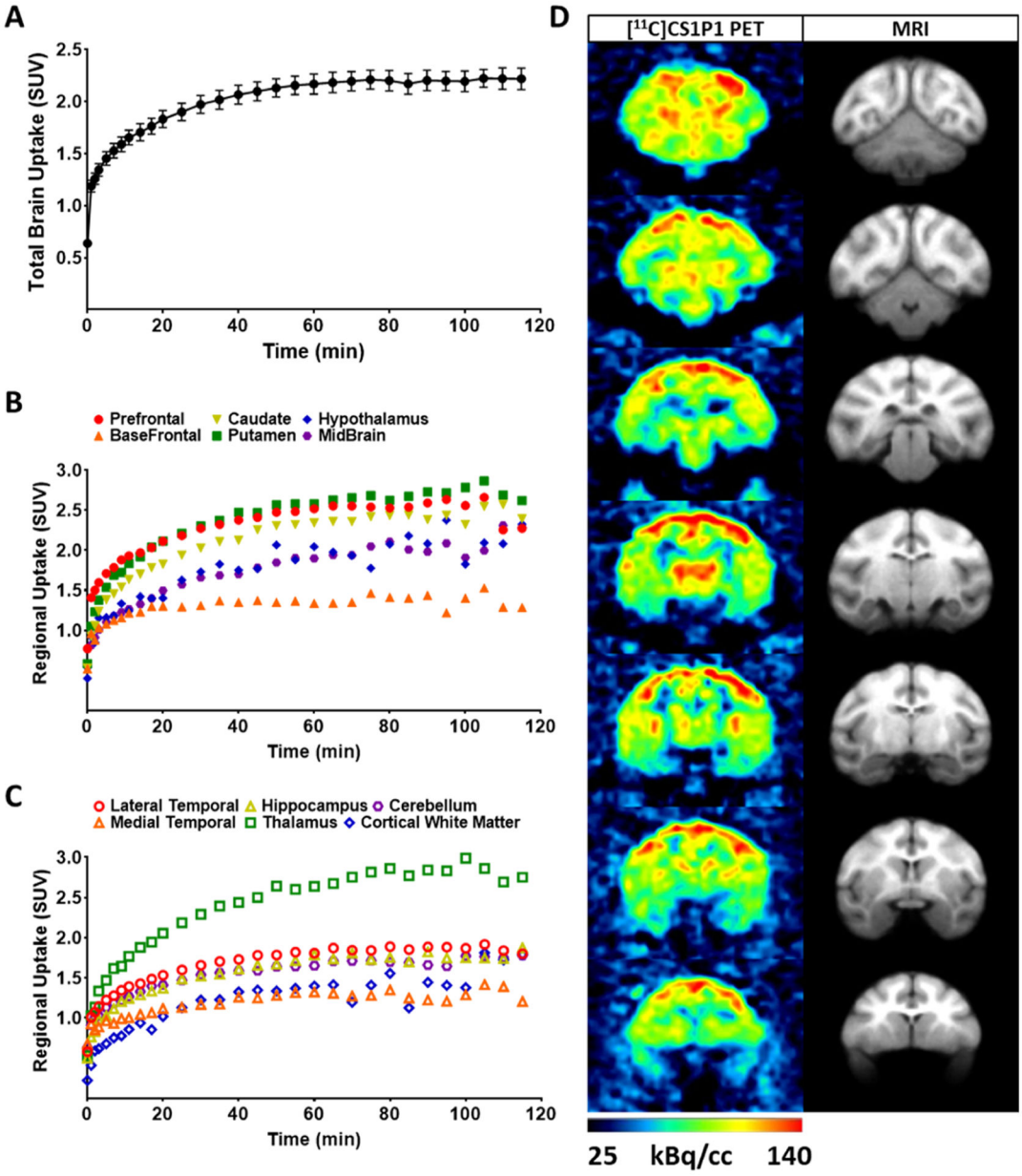

Figure 4.

In vivo brain uptake [^{11}C]CS1P1 in the non-human primate brain. (A) Average of standard uptake of total [^{11}C]CS1P1 in six NHP brains; (B) average uptake of [^{11}C]CS1P1 in different regions including prefrontal, basal frontal, caudate, putamen, hypothalamus, and midbrain in six NHP brains; (C) average uptake of [^{11}C]CS1P1 in different regions including lateral and medial temporal, hippocampus, thalamus, cerebellum, and cortical white matter in six NHP brains; and (D) representative different frames of PET images and MRI images of [^{11}C]CS1P1 in the selected NHP brain.

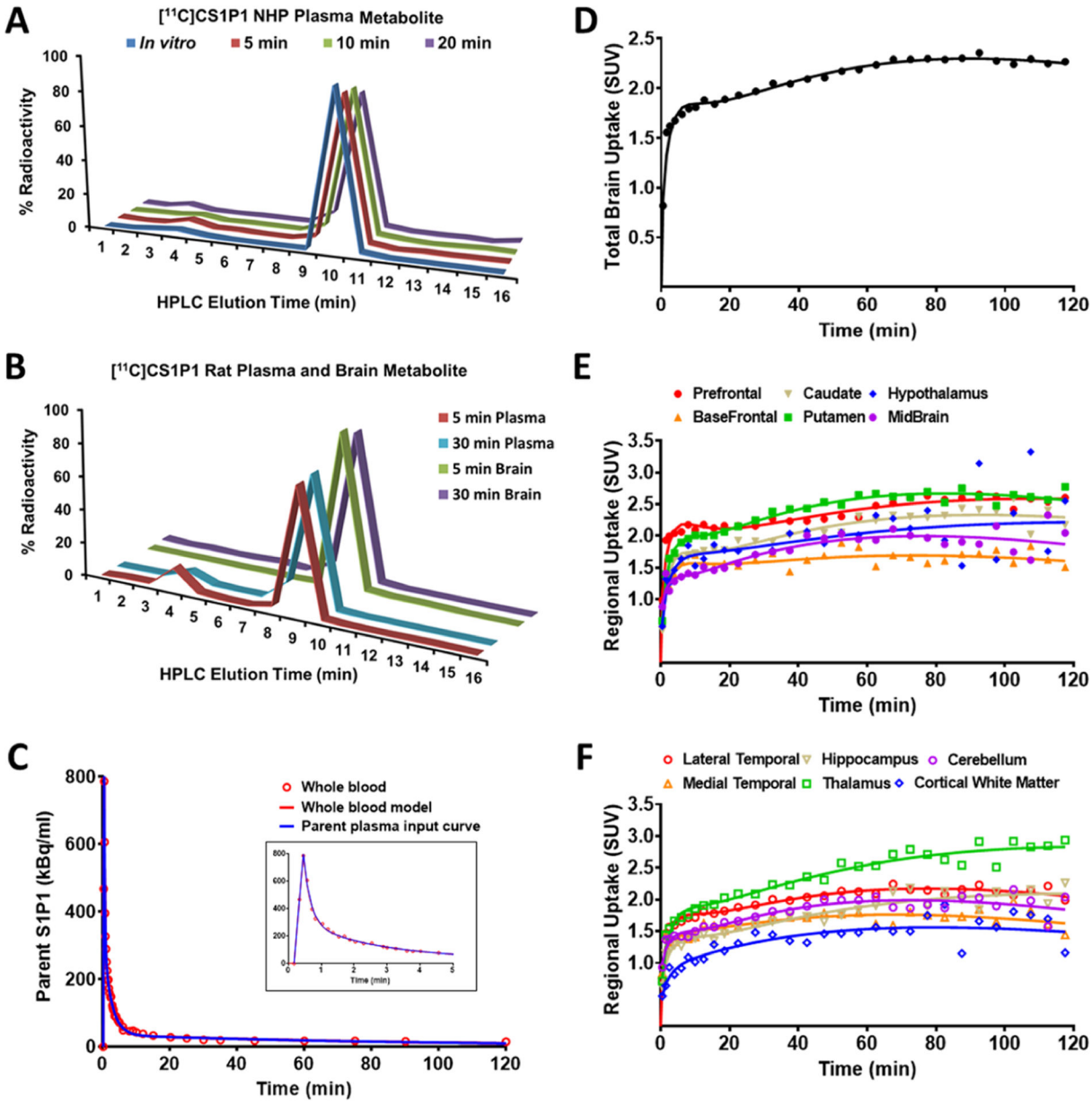

Figure 5.

[11C]CS1P1 metabolism analysis and kinetic model fitting of [11C]CS1P1 uptake in the NHP brain. (A,B) *Ex vivo* [11C]CS1P1 metabolism analysis in rodent and non-human primate plasma and brain: (A) [11C]CS1P1 plasma metabolism analysis in NHP showed no major metabolites in NHP blood; (B) [11C]CS1P1 plasma metabolism analysis in rat showed a small amount of metabolite in rat blood at 5 min and no to very low amount in later time point, [11C]CS1P1 brain metabolism analysis in rat showed no metabolites in the homogenates of the rat brain. (C) Time-activity curves for NHP whole blood and plasma: whole-blood, whole-blood fit to three exponential model to define the blood curve, and the parent mcPIF is shown. (D–F) Kinetic model fitting of [11C]CS1P1 uptake in the

NHP brain: (D) 2-tissue compartmental model fit to the total brain uptake; (E–F) 2-tissue compartment model regression against time-activity curves of select brain regions.

Table 1.

Summary of [^{11}C]CS1P1 PET Studies in Non-Human Primates

mean SUV (0–120 min)	NHP1	NHP2	NHP3	NHP4	NHP5	NHP6	mean (*n* = 6)	CV, %
test	2.03	1.69	1.64	2.10	2.10	1.88	1.91	10.70
retest	1.98	1.52	1.80	2.13	2.10	1.82	1.89	12.01
% mean change	2.35	9.88	9.42	1.23	0.19	3.52	0.91	
TRV, %	0.60	2.60	2.25	0.31	0.05	0.90	0.23	